# An Experimental Evidence of a Metal–Metal Bond in μ-Carbonylhexacarbonyl[μ-(5-oxofuran-2(5*H*)-ylidene-κ*C*,κ*C*)]-dicobalt(*Co–Co*)[$Co_2(CO)_6(\mu\text{-}CO)(\mu\text{-}C_4O_2H_2)$]

by **Riccardo Bianchi**

Centro CNR per lo Studio delle Relazioni tra Struttura e Reattività Chimica, Via Venezian 21, I-20133 Milano

and **Giuliana Gervasio*** and **Domenica Marabello**

Dipartimento di Chimica I.F.M. dell'Università, Via P. Giuria 7, I-10125 Torino

The orthorhombic crystal structure of $[Co_2(CO)_6(\mu\text{-}CO)(\mu\text{-}C_4O_2H_2)]$ (**1**) was determined at 150 K (*Fig. 1*). Two C–H···O bonds connect the molecules, forming waving ribbons along the *b* axis. The experimental electron density, determined with the aspherical-atom formalism, was analyzed with the topological theory of molecular structure. The presence of the Co–Co bond critical point indicates for the first time the existence of a metal–metal bond in a system with bridged ligands. The bond critical properties of the intramolecular bonds and of the intermolecular interactions show features similar to those found in $[Mn_2(CO)_{10}]$, confirming our previously established bonding classification for organometallic and coordination compounds.

**1. Introduction.** – Different hypotheses were made on the existence and nature (straight or bent) of a metal–metal bond in systems with bridging ligands. Early, in the solid state, the bridged isomer of $[Co_2(CO)_8]$ was described as containing a Co–Co single bond on the basis of the 'effective atomic number' (EAN) rule [1]. Subsequent theoretical calculations were controversial and supported both models involving the absence [2] or the presence [3] of a metal–metal bond between the Co-atoms. An experimental density study [4] yielded no definitive answer about the existence of the bond.

A more recent theoretical analysis [5] of the topology of $[Co_2(CO)_8]$ electron density, calculated at the *ab initio* rescricted *Hartree-Fock* (RHF) level by means of *Huzinaga*'s (13s7p5d/4s3p3d) and (6s3p/3s2p) Gaussian contractions for Co- and for C- and O-atoms, respectively, showed a ring critical point close to the Co–Co midpoint. The conclusion of this study was: 'although some constructive interference occurs between the two cobalt atoms, it is not sufficient to produce a Co–Co bond' and 'all of the formal bonds between the two cobalt atoms occur through the bridging carbonyls'.

Another topological analysis [6] of the theoretical electrondensity of $[Co_2(\eta^5\text{-}C_5H_5)_2(\mu\text{-}NO)_2]$ (Co–Co separation of 2.37 Å), by means of the *Williamson* and *Hall* split-valence basis set for the Co-atom, showed that, at certain geometries (bent $Co_2N_2$ ring) and levels of electron correlation, there exists a Co–Co bond, but at other geometries (planar $Co_2N_2$ ring) and levels of electron correlation, the Co–Co bond critical point vanishes to be replaced by a $Co_2N_2$ ring critical point. Thus, the authors concluded that, as in $[Co_2(CO)_8]$ (Co–Co separation of 2.53 Å), the Co–Co interaction is near the region of change from having to not having a bond. In fact,

the theoretical electron density of $[Co_2(CO)_8]$, computed with a Co–Co distance of 2.37 Å, showed a $(3,-1)$ bond critical point between the Co-atoms. Also, it was concluded [5] that 'this behavior is an indication of the flat nature of the electron density inside the $Co_2(\mu\text{-}C)_2$ ring', and that 'the density need not change much to alter the nature of the critical point between the cobalt atoms'.

In this paper, we continue the experimental study [7] of metal–metal and metal-ligand bonds in terms of topological properties [8] of the electron density, determined by a multipole refinement procedure [9]. The subject of this paper is a cobalt carbonyl complex of formula $[Co_2(CO)_6(\mu\text{-}CO)(\mu\text{-}C_4O_2H_2)]$ (**1**; $C_4O_2H_2$ = 5-oxofuran-2(5*H*)-ylidene) [10]. Complex **1** is intermediate in the Co–Co separation (2.42 Å) with respect to $[Co_2(CO)_8]$ and $[Co_2(\eta^5\text{-}C_5H_5)_2(\mu\text{-}NO)_2]$, and has two bridging ligands, a CO group and a $\gamma$-lactone ring. It is also an example of complexes where an organic ring, perpendicular to a metal–metal bond, joins two fragments of a molecule. Complex **1** is parent to a series of derivatives obtained by substitution of two CO ligands with diamine [11], dithioether [12], or diphosphine [13] ligands and was synthetized from $[Co_2(CO)_8]$ and acetylene under CO pressure [11][14]. Because of its good stability, besides other features, **1** was preferred over $[Co_2(CO)_8]$ for the present electron-density study. Complex **1** is an intermediate in the catalytic cycle that starts from $[Co_2(CO)_8]$, acetylene, and CO to yield bis[furandiones] [15].

$[Co_2(CO)_6(\mu\text{-}CO)(\mu\text{-}C_4O_2H_2)]$ (**1**) crystallizes in two polymorphic phases (orthorhombic and triclinic). The structural analysis of the triclinic form was published elsewhere [10], and here we report the structural results and the experimental electron-density analysis of the orthorhombic form.

**2. Results.** – 2.1. *Structural Properties.* In the molecule of $[Co_2(CO)_6(\mu\text{-}CO)(\mu\text{-}C_4O_2H_2)]$ (**1**), two $Co(CO)_3$ moieties are joined by a bridging CO group and by a $\gamma$-lactone-derived ligand (*Fig. 1*). In this $\gamma$-lactone ligand, the C(8)–C(9) bond corresponds formally to a double bond and the lactone ring is almost planar (mean deviation from planarity 0.0021 Å). It lies on the molecular *m* plane and forms an angle of 88° with the Co–Co bond. Each Co-atom is bonded to three terminal CO groups oriented in an eclipsed configuration. The angle between the two $Co_2C(4)$ and $Co_2C(6)$ triangles is 111°, and a slight asymmetry occurs between the Co–C(4)–O(4) angles (*Table 1*). Bond distances and angles, intermolecular O···O and O···C interactions (< 3.4 Å), and O···H H-bonds from POP refinement are listed in *Table 1*. The atomic fractional coordinates and the anisotropic and isotropic thermal parameters of the multipolar refinement are listed in *Table 2*.

2.2. *Experimental Electron Density.* The residual map (based on $F_{observed} - F_{multipole}$) shows no significant features (see, *e.g. Fig. 2,a*) and the largest peak (close to the Co(2) atom) is 0.20 eÅ$^{-3}$. The average standard deviation of the total density, which is representative of the error in the difference density at positions away from the atoms, is 0.1 eÅ$^{-3}$. That all the features in the residual map are below $3\sigma$ indicates that the POP model used (see *Exper. Part*) in the refinement is adequate. Net atomic charges, defined as the atomic number *Z* minus the sum of the core and valence populations, are given in *Table 3*.

The static deformation density map (*Fig. 2,b*) shows the electron accumulation due to bonding between the atoms. We observe a flat peak on the midpoint of the Co–Co

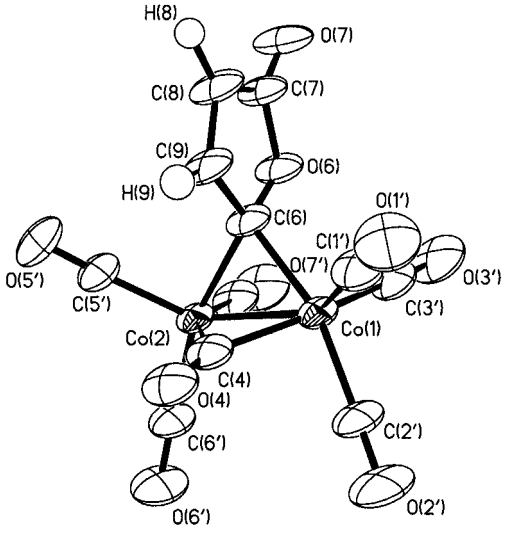


Fig. 1. *ORTEP Plot* (30% probability) *of* $[Co_2(CO)_6(\mu\text{-}CO)(\mu\text{-}C_4O_2H_2)]$ (**1**)

bond (0.43(6) eÅ$^{-3}$) and maxima between other bonded atoms. The shape and intensity of the electron density are well-correlated with the bond lengths. The broad diffuse peaks along the bonds of the Co(1)Co(2)C(4) ring are well-distinguishable from the well-shaped peaks on the shorter CO bonds (see *Fig. 2,b*), and the presence of peaks in the lone-pair regions of the O-atoms is noticeable.

2.3. *Topological Analysis.* The topology of the experimental electron density $\rho(\boldsymbol{r})$ and its Laplacian $\nabla^2\rho(\boldsymbol{r})$ from the POP model is related to chemical concepts by the quantum theory of atoms in molecules (QTAM) [8a]. This theory identifies the existence of a $(3,-1)$ critical point (BCP) along a line of maximum density (bond path) with the presence of bonding between the two atoms so linked. At the BCP, the gradient of the density vanishes, *i.e.* $\nabla^2\rho(\boldsymbol{r})=0$, and the sum of the three eigenvalues (two negative, $\lambda_1$ and $\lambda_2$, and one positive, $\lambda_3$) of the density *Hessian* matrix yields the Laplacian value $\nabla^2\rho_b$. The topology of the $\nabla^2\rho(\boldsymbol{r})$ allows the study of localized bonding and nonbonding pairs and the characterization of local concentrations ($\nabla^2\rho(\boldsymbol{r})<0$) of the electron density and its depletion ($\nabla^2\rho(\boldsymbol{r})>0$). The number and properties of the local $\nabla^2\rho(\boldsymbol{r})$ maxima and minima in the valence shell charge concentration (VSCC) of the bonded atoms depend on the linked atoms themselves. In 'shared' interactions, where $\nabla^2\rho(\boldsymbol{r})<0$, there is a lowering of the potential-energy density $V(\boldsymbol{r})$ associated with a concentration in charge between the nuclei along the bond path. 'Closed-shell' interactions, where $\nabla^2\rho_b>0$, are dominated by the kinetic-energy density $G(\boldsymbol{r})$ in the region of the interatomic surface. Additional information about a chemical bond is available from the total electronic-energy density $E_b^e=G_b+V_b$, where $G_b$ and $V_b$ are the experimental values of the kinetic- and potential-energy density, respectively, at the BCP. They cannot be rigorously calculated from a knowledge of only density, and they were thus obtained by means of an empirical functional theory from *Abramov* [16] and *Espinosa et al.* [17].

Table 1. *Relevant Bond Distances [Å] and Angles [°] and Intermolecular O ··· H, O ··· O, and O ··· C Interactions from the POP Refinement*

| Intramolecular bond distances | | Intramolecular bond angles | | Intermolecular interactions[a]) | |
|---|---|---|---|---|---|
| Co(1)–Co(2) | 2.4222(3) | Co(2)–Co(1)–C(1′) | 138.62(8) | O(1′) ··· O(2′)$^{I}$ | 3.104(9)*[b]) |
| Co(1)–C(1) | 1.809(3) | Co(2)–Co(1)–C(2′) | 107.80(9) | O(1′) ··· O(3′)$^{II}$ | 3.259(7)*[b]) |
| Co(1)–C(2′) | 1.834(3) | Co(2)–Co(1)–C(3′) | 105.43(8) | O(1″) ··· O(6′)$^{III}$ | 3.277(8)*[b]) |
| Co(1)–C(3′) | 1.855(3) | Co(2)–Co(1)–C(4) | 50.96(6) | O(2″) ··· O(5′)$^{III}$ | 3.181(8)*[b]) |
| Co(1)–C(4) | 1.921(2) | Co(2)–Co(1)–C(6) | 52.47(5) | O(2′) ··· O(7′)$^{IV}$ | 3.181(8)*[b]) |
| Co(1)–C(6) | 1.984(2) | Co(1)–Co(2)–C(4) | 50.90(6) | O(2′) ··· O(7)$^{II}$ | 3.227(8) |
| Co(2)–C(4) | 1.922(2) | Co(1)–Co(2)–C(5′) | 136.80(9) | O(3″) ··· O(6′)$^{VI}$ | 3.034(7)*[b]) |
| Co(2)–C(5′) | 1.809(3) | Co(1)–Co(2)–C(6) | 52.34(5) | O(4′) ··· O(6′)$^{III}$ | 3.048(6) |
| Co(2)–C(6) | 1.987(2) | Co(1)–Co(2)–C(6′) | 108.30(8) | O(7′) ··· O(6)$^{IX}$ | 3.280(6) |
| Co(2)–C(6′) | 1.824(3) | Co(1)–Co(2)–C(7′) | 100.50(8) | O(2′) ··· C(8)$^{V}$ | 3.359(8)*[b]) |
| Co(2)–C(7′) | 1.851(3) | Co(1)–C(4)–Co(2) | 78.13(8) | O(3′) ··· C(7)$^{II}$ | 3.284(6) |
| C(1′)–O(1′) | 1.135(6) | Co(1)–C(6)–Co(2) | 75.18(7) | O(4) ··· C(5′)$^{III}$ | 3.181(4) |
| C(2′)–O(2′) | 1.135(7) | Co(1)–C(1′)–O(1′) | 177.9(4) | O(4) ··· O(5′)$^{III}$ | 3.259(6) |
| C(3′)–O(3′) | 1.136(5) | Co(1)–C(2′)–O(2′) | 178.4(5) | O(4) ··· C(6′)$^{III}$ | 3.034(4)*[b]) |
| C(4)–O(4) | 1.174(4) | Co(1)–C(3′)–O(3′) | 177.7(3) | O(6′) ··· C(8)$^{Viii}$ | 3.213(5)*[b]) |
| C(5′)–O(5′) | 1.132(6) | Co(1)–C(4)–O(4) | 142.3(2) | O(7′) ··· C(7)$^{IX}$ | 3.007(5)*[b]) |
| C(6′)–O(6′) | 1.142(5) | Co(2)–C(4)–O(4) | 139.5(2) | O(7′) ··· C(8)$^{IX}$ | 3.260(6) |
| C(7′)–O(7′) | 1.136(6) | Co(2)–C(5′)–O(5′) | 177.9(4) | O(7) ··· C(1′)$^{IX}$ | 3.355(4) |
| C(6)–O(6) | 1.410(3) | Co(2)–C(6′)–O(6′) | 175.7(3) | O(7) ··· C(2′)$^{IX}$ | 3.055(5)*[b]) |
| O(6)–C(7) | 1.377(3) | Co(2)–C(7′)–O(7′) | 177.5(3) | O(7) ··· C(3′)$^{IX}$ | 3.192(5) |
| C(7)–O(7) | 1.209(4) | O(6)–C(6)–C(9) | 105.0(2) | O(7) ··· C(9)$^{X}$ | 3.175(4) |
| C(7)–C(8) | 1.460(4) | C(6)–O(6)–C(7) | 109.9(2) | O(6′) ··· H(8)$^{VIII}$ | 2.92(6) |
| C(8)–C(9) | 1.348(4) | O(6)–C(7)–O(7) | 120.8(3) | O(4) ··· H(8)$^{VII}$ | 2.55(7)*[b]) |
| C(6)–C(9) | 1.464(3) | O(6)–C(7)–C(8) | 107.9(2) | O(7) ··· H(9)$^{X}$ | 2.32(6)*[b]) |
| C(8)–H(8) | 1.07(7) | C(7)–C(8)–C(9) | 107.2(2) | | |
| C(9)–H(9) | 0.97(6) | C(6)–C(9)–C(8) | 110.1(2) | | |
| | | C(7)–C(8)–H(8) | 129(3) | | |
| | | C(8)–C(9)–H(9) | 122(3) | | |

[a]) The roman numbers refer to the following symmetry operations: I: $-0.5-x$, $-y$, $0.5+z$; II: $-0.5+x$, $-0.5-y$, $2-z$; III: $-0.5+x$, $0.5-y$, $2-z$; IV: $-x$, $0.5+y$, $1.5-z$; V: $-0.5-x$, $-y$, $-0.5+z$; VI: $-x$, $-0.5+y$, $1.5-z$; VII: $-x$, $0.5+y$, $2.5-z$; VIII: $0.5-x$, $-y$, $-0.5+z$; IX: $0.5+x$, $-0.5-y$, $2-z$; X: $-x$, $-0.5+y$, $2.5-z$.

[b]) Contacts marked with an asterisk indicate atomic interactions where bond paths and BCPs were found from the topological analysis of the experimental $\rho(\mathbf{r})$ (see *Table 5*).

The covalent bonds show relatively large values of $\rho_b$ (the value of $\rho(\boldsymbol{r})$ at the BCP) and large negative values of $\nabla^2 \rho_b$. These 'shared' interactions have a negative $E_b^e$, being dominated by a large negative $V_b$ associated with charge concentration in the internuclear region. Instead, the ionic bonds have a relatively low $\rho_b$ and a positive $\nabla^2 \rho_b$ as the density contracts away from the contact region of the interacting atoms. These 'closed-shell' interactions are dominated by the kinetic energy in the region of the BCP with $G_b$ slightly greater than $|V_b|$ and with $E_b^e$ positive and close to zero. Previous topological analyses of the experimental electron density on a number of organometallic and coordination compounds [7b] suggested that metal–metal bonds and metal-ligand bonds have topological properties intermediate between covalent and ionic bonds.

Table 2. *Atomic Fractional Coordinates and Thermal Parameters* [Å$^2 \cdot 10^2$] *from the POP Refinement.* $T(\text{aniso}) = \exp[-2\pi^2(U_{11}h^2a^{*2} + \cdots + 2U_{23}klb^*c^*)]$, $T(\text{iso}) = \exp[-2U(2\pi\sin\theta/\lambda)^2]$

| | $x$ | $y$ | $z$ | $U_{11}$ | $U_{22}$ | $U_{33}$ | $U_{12}$ | $U_{13}$ | $U_{23}$ |
|---|---|---|---|---|---|---|---|---|---|
| Co(1) | −0.09770(2) | −0.02165(2) | 0.96428(2) | 2.27(1) | 2.41(1) | 2.34(1) | 0.047(7) | −0.213(6) | 0.152(7) |
| Co(2) | 0.14152(2) | 0.03464(2) | 0.98165(1) | 2.25(1) | 2.20(1) | 2.27(1) | 0.000(6) | 0.058(6) | 0.034(6) |
| C(1′) | −0.2516(2) | −0.0239(3) | 1.0372(2) | 3.09(8) | 3.50(9) | 4.3(1) | 0.05(8) | 0.42(8) | 0.0(1) |
| O(1′) | −0.3504(5) | −0.0245(6) | 1.0805(4) | 4.0(1) | 5.9(2) | 6.5(2) | −0.3(2) | 1.9(1) | −0.3(2) |
| C(2′) | −0.1643(3) | 0.0618(3) | 0.8573(2) | 4.2(1) | 3.8(1) | 3.7(1) | −0.23(9) | −1.26(9) | 1.00(9) |
| O(2′) | −0.2032(8) | 0.1154(6) | 0.7914(5) | 7.6(3) | 5.8(2) | 5.3(2) | −0.6(2) | −2.9(2) | 2.2(2) |
| C(3′) | −0.0984(3) | −0.1806(2) | 0.9052(2) | 3.65(9) | 3.18(9) | 3.55(9) | −0.04(8) | −0.75(8) | −0.53(7) |
| O(3′) | −0.1005(6) | −0.2796(4) | 0.8719(4) | 5.8(2) | 4.0(1) | 5.7(2) | 0.4(2) | −1.6(2) | −1.7(1) |
| C(4) | −0.0184(2) | 0.1350(2) | 1.0095(2) | 3.20(7) | 2.44(6) | 3.14(7) | 0.23(6) | 0.01(6) | −0.05(6) |
| O(4) | −0.0471(4) | 0.2380(3) | 1.0361(3) | 4.2(1) | 2.88(9) | 4.7(1) | 0.72(9) | 0.0(1) | −0.5(1) |
| C(5′) | 0.2565(3) | 0.0743(3) | 1.0800(2) | 3.6(1) | 3.47(9) | 3.5(1) | −0.40(8) | −0.66(8) | −0.09(8) |
| O(5′) | 0.3279(6) | 0.0954(5) | 1.1427(4) | 5.5(2) | 6.0(2) | 4.7(2) | −1.1(2) | −2.0(2) | −0.6(2) |
| C(6′) | 0.1822(2) | 0.1564(3) | 0.8918(2) | 3.36(9) | 3.50(9) | 3.19(8) | −0.23(7) | 0.30(7) | 0.75(8) |
| O(6′) | 0.1997(5) | 0.2356(5) | 0.8363(3) | 5.2(2) | 5.1(2) | 4.5(2) | −0.6(2) | 0.6(1) | 2.0(1) |
| C(7′) | 0.2231(2) | −0.0988(2) | 0.9155(2) | 3.18(8) | 3.23(9) | 3.62(9) | 0.40(7) | 0.62(7) | −0.43(8) |
| O(7′) | 0.2684(5) | −0.1825(5) | 0.8743(4) | 5.0(2) | 4.7(2) | 5.8(2) | 1.0(2) | 1.6(2) | −1.4(2) |
| C(6) | 0.0340(2) | −0.0867(2) | 1.0619(1) | 2.77(7) | 2.71(7) | 2.34(6) | 0.27(5) | 0.05(5) | 0.00(5) |
| C(7) | 0.0687(2) | −0.2657(3) | 1.1527(2) | 3.05(8) | 3.25(9) | 3.21(8) | 0.36(7) | 0.32(6) | 1.00(7) |
| C(8) | 0.0272(2) | −0.1637(3) | 1.2185(2) | 3.59(9) | 4.2(1) | 2.38(7) | 0.34(8) | 0.23(6) | 0.63(8) |
| C(9) | 0.0074(2) | −0.0584(2) | 1.1642(1) | 3.24(8) | 3.52(9) | 2.31(6) | 0.33(7) | 0.13(6) | −0.02(6) |
| O(6) | 0.0724(3) | −0.2163(2) | 1.0602(2) | 3.40(9) | 2.68(7) | 2.70(7) | 0.37(7) | 0.23(7) | 0.28(6) |
| O(7) | 0.0975(4) | −0.3760(3) | 1.1677(3) | 4.4(1) | 3.9(1) | 4.5(1) | 0.8(1) | 0.7(1) | 1.8(1) |
| H(8) | 0.017(6) | −0.165(6) | 1.296(5) | 4.0(1)[a] | | | | | |
| H(9) | −0.023(5) | 0.022(6) | 1.193(4) | 5.0(1)[a] | | | | | |

[a]) $U$ value.

Table 3. *Net Atomic Charges* [e] *from the POP Refinement*

| | Charge (e.s.d.s) | | Charge (e.s.d.s) |
|---|---|---|---|
| Co(1) | −0.3(3) | C(6′) | −0.28(7) |
| Co(2) | −0.3(3) | O(6′) | 0.32(5) |
| C(1′) | −0.28(7) | C(7′) | −0.28(7) |
| O(1′) | 0.32(5) | O(7′) | 0.32(5) |
| C(2′) | −0.28(7) | C(6) | −0.1(1) |
| O(2′) | 0.32(5) | C(7) | −0.28(7) |
| C(3′) | −0.28(7) | C(8) | −0.2(1) |
| O(3′) | 0.32(5) | C(9) | −0.1(2) |
| C(4) | −0.28(7) | O(6) | 0.20(7) |
| O(4) | 0.32(5) | O(7) | 0.18(9) |
| C(5′) | −0.28(7) | H(8) | 0.4(1) |
| O(5′) | 0.32(5) | H(9) | 0.2(1) |

The properties of the experimental electron density at the critical points for complex **1** are reported in *Tables 4* and *5*. *Figs. 3* and *4* show the experimental electron density of $[Co_2(CO)_6(\mu\text{-}CO)(\mu\text{-}C_4O_2H_2)]$ (**1**) and its Laplacian in the Co(1)Co(2)C(4), Co(1)Co(2)C(6), and $\gamma$-lactone planes, respectively.

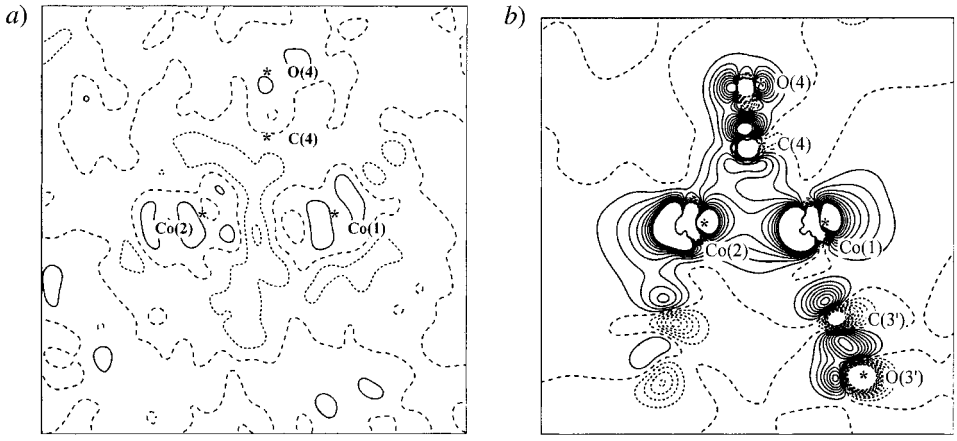


Fig. 2. a) *Residual density and* b) *model static-deformation density maps in the plane defined by the Co(1), Co(2), and C(4) atoms of* **1**. The contour interval is 0.10 eÅ$^{-3}$. Solid lines (–) represent a positive, short dashed lines (- - -) a negative, and wide dashed lines (– – –) a zero contour.

*The Co–C Bonds.* The Co–C bonds of **1** are characterized by a relatively low $\rho_b$ of 0.92 eÅ$^{-3}$ av. and by a positive Laplacian (9.4 eÅ$^{-5}$ av.); therefore, they must be classified as 'closed-shell'. It is interesting to note the trend of the Co–$C_{CO}$ bond lengths and of the corresponding $\rho_b$ values. From *Table 4*, we have $R_e$ and $\rho_b$ average values of 1.853(4) Å and 0.81(6) eÅ$^{-3}$ for the equatorial Co(1)–C(3′) and Co(2)–C(7′) bonds, of 1.829(4) Å and 0.94(7) eÅ$^{-3}$ for the equatorial Co(1)–C(2′) and Co(2)–C(6′) bonds, and of 1.809(4) Å and 1.10(8) eÅ$^{-3}$ for the axial Co(1)–C(1′) and Co(2)–C(5′) bonds. The electron density at the BCPs has a reverse trend with respect to the corresponding bond distance. The values reported above suggest an easier substitution of equatorial COs than of axial COs. In fact, normally, substitution reactions of equatorial COs with N⌒N, S⌒S, and P⌒P ligands occur [11–13]. Furthermore, the differences of $R_e$ and $\rho_b$ values between the equatorial COs indicate a greater *trans* influence of the CO(4) ligand with respect to the $\gamma$-lactone-ring ligand.

As found in $[Co_2(CO)_6(AsPh_3)_2]$ [18], the Co–$C_{CO}$ BCPs of **1** are closer to the C-atom, while in $[Mn_2(CO)_{10}]$ the BCPs are very close to the middle of the Mn–C bonds [7b]. The Co–C BCPs of the two bridges of **1** lie closer to the C-atoms with respect to those of the terminal COs, indicating an expansion of the Co basin towards the C(4) and C(6) atoms. The Co–C BCPs of the two bridges are situated on the corresponding planes defined by the $Co_2C(4)$ and $Co_2C(6)$ triangles, and they are shifted, on average, by 0.12 Å towards the center of the triangles. This could indicate a slight electron deficiency in the two $Co_2C(4)$ and $Co_2C(6)$ rings.

The $G_b$ and $|V_b|$ values of the Co–C bonds are comparable, and the resulting energy densities $E_b^e$ have slightly negative values.

These metal-ligand interactions of **1** exhibit $\rho_b$, $\nabla^2\rho_b$, $G_b$, $V_b$, and $E_b^e$ values in agreement with the scheme suggested in our previous report on $[Mn_2(CO)_{10}]$ [7b].

*The C–O Bonds.* In complex **1**, three types of C–O bonds are present: the C≡O carbonyl ligands (six terminal COs, and one bridging CO) and the C=O and C–O bonds of the $\gamma$-lactone ring.

Table 4. *Bond Critical-Point Properties from the POP Model.* $R_e$ = distance between atoms X and Y; $R_b$ = bond path length; $R_x$ = distance between atom X and the BCP.

| X-Y | $R_e$ [Å] | $R_b$ [Å] | $R_x$ [Å] | $\rho_b$ [eÅ$^{-3}$] | $\nabla^2\rho_b$ [eÅ$^{-5}$] | $\lambda_1$ [eÅ$^{-5}$] | $\lambda_2$ [eÅ$^{-5}$] | $\lambda_3$ [eÅ$^{-5}$] | $G_b$ [hartree Å$^{-3}$] | $G_b/\rho_b$ [hartree e$^{-1}$] | $V_b$ [hartree Å$^{-3}$] | $E_b^e$ [hartree Å$^{-3}$] |
|---|---|---|---|---|---|---|---|---|---|---|---|---|
| Intramolecular bond critical points: | | | | | | | | | | | | |
| Co(1)–Co(2) | 2.4222(3) | 2.4528 | 1.2119 | 0.76(6) | 2.0(3) | – 1.8 | – 1.0 | 4.8 | 0.60 | 0.79 | – 1.06 | – 0.46 |
| Co(1)–C(1′) | 1.809(3) | 1.829 | 0.972 | 1.18(5) | 8.6(6) | – 5.5 | – 5.0 | 19.1 | 1.46 | 1.24 | – 2.32 | – 0.86 |
| Co(1)–C(2′) | 1.834(3) | 1.843 | 0.963 | 0.93(5) | 12.2(6) | – 4.5 | – 3.4 | 20.1 | 1.28 | 1.38 | – 1.71 | – 0.43 |
| Co(1)–C(3′) | 1.855(3) | 1.879 | 0.945 | 0.75(4) | 15.1(5) | – 4.5 | – 3.3 | 22.9 | 1.20 | 1.60 | – 1.35 | – 0.15 |
| Co(1)–C(4) | 1.921(2) | 1.958 | 1.012 | 0.84(4) | 8.5(3) | – 3.4 | – 2.2 | 14.1 | 1.00 | 1.19 | – 1.40 | – 0.40 |
| Co(1)–C(6) | 1.984(2) | 2.038 | 1.031 | 0.90(4) | 5.4(3) | – 4.1 | – 2.8 | 12.3 | 1.00 | 1.03 | – 1.47 | – 0.54 |
| Co(2)–C(4) | 1.922(2) | 1.963 | 1.024 | 0.97(6) | 6.5(3) | – 4.1 | – 3.3 | 13.9 | 1.08 | 1.10 | – 1.68 | – 0.60 |
| Co(2)–C(5′) | 1.809(3) | 1.828 | 0.963 | 1.02(6) | 10.9(8) | – 5.2 | – 3.7 | 19.8 | 1.34 | 1.31 | – 1.92 | – 0.58 |
| Co(2)–C(6) | 1.987(2) | 2.023 | 1.049 | 0.83(4) | 5.5(2) | – 3.8 | – 1.9 | 11.2 | 0.85 | 1.02 | – 1.31 | – 0.46 |
| Co(2)–C(6′) | 1.824(3) | 1.872 | 0.953 | 0.95(5) | 12.9(5) | – 5.5 | – 3.9 | 22.4 | 1.34 | 1.41 | – 1.78 | – 0.44 |
| Co(2)–C(7′) | 1.851(3) | 1.867 | 0.968 | 0.87(5) | 12.3(3) | – 4.3 | – 3.4 | 20.0 | 1.21 | 1.39 | – 1.56 | – 0.35 |
| C(1′)–O(1′) | 1.135(6) | 1.142 | 0.448 | 3.8(2) | – 52(5) | – 39 | – 33 | 20 | 5.01 | 1.32 | – 13.67 | – 8.66 |
| C(2′)–O(2′) | 1.135(7) | 1.135 | 0.433 | 4.0(2) | – 66(6) | – 51 | – 35 | 20 | 5.02 | 1.26 | – 14.67 | – 9.65 |
| C(3′)–O(3′) | 1.136(5) | 1.141 | 0.399 | 3.7(2) | – 36(6) | – 42 | – 36 | 42 | 5.44 | 1.47 | – 13.39 | – 7.95 |
| C(4)–O(4) | 1.174(4) | 1.179 | 0.528 | 3.4(1) | – 34(3) | – 31 | – 28 | 25 | 4.59 | 1.35 | – 11.57 | – 6.98 |
| C(5′)–O(5′) | 1.132(6) | 1.136 | 0.434 | 3.9(2) | – 56(8) | – 42 | – 36 | 22 | 5.16 | 1.32 | – 14.23 | – 9.07 |
| C(6′)–O(6′) | 1.142(5) | 1.150 | 0.473 | 3.7(2) | – 45(4) | – 36 | – 32 | 23 | 5.02 | 1.36 | – 13.18 | – 8.16 |
| C(7′)–O(7′) | 1.136(6) | 1.137 | 0.442 | 3.6(2) | – 50(4) | – 38 | – 32 | 20 | 4.47 | 1.24 | – 12.43 | – 7.96 |
| C(6)–O(6) | 1.410(3) | 1.413 | 0.580 | 1.8(1) | – 11(3) | – 13 | – 12 | 14 | 1.63 | 0.90 | – 4.03 | – 2.40 |
| C(7)–O(6) | 1.377(3) | 1.382 | 0.571 | 1.9(1) | – 17(5) | – 16 | – 15 | 14 | 1.55 | 0.82 | – 4.29 | – 2.74 |
| C(7)–O(7) | 1.209(4) | 1.221 | 0.547 | 3.1(1) | – 22(4) | – 29 | – 21 | 27 | 4.27 | 1.38 | – 10.09 | – 5.82 |
| C(7)–C(8) | 1.460(4) | 1.473 | 0.752 | 1.96(9) | – 13(1) | – 14 | – 13 | 14 | 1.86 | 0.95 | – 4.63 | – 2.77 |
| C(8)–C(9) | 1.348(4) | 1.354 | 0.693 | 2.3(1) | – 17(2) | – 18 | – 13 | 14 | 2.43 | 1.06 | – 6.05 | – 3.62 |
| C(6)–C(9) | 1.464(3) | 1.471 | 0.764 | 2.04(8) | – 13(3) | – 15 | – 13 | 15 | 2.03 | 1.00 | – 4.97 | – 2.94 |
| C(8)–H(8) | 1.07(7) | 1.077 | 0.780 | 1.6(1) | – 14(5) | – 18 | – 18 | 22 | 1.11 | 0.69 | – 3.19 | – 2.08 |
| C(9)–H(9) | 0.97(6) | 0.974 | 0.567 | 2.1(1) | – 22(4) | – 18 | – 17 | 13 | 1.74 | 0.83 | – 5.02 | – 3.28 |
| Intramolecular ring critical points: | | | | | | | | | | | | |
| Co(1)–Co(2)–C(4) | | | | 0.73(5) | 3.0(2) | – 1.9 | 1.8 | 3.1 | | | | |
| Co(1)–Co(2)–C(6) | | | | 0.74(6) | 2.1(2) | – 2.2 | 1.5 | 2.8 | | | | |
| C(6)–O(6)–C(7)–C(8)–C(9) | | | | 0.45(2) | 5.9(2) | – 1.5 | 3.4 | 3.9 | | | | |

The C≡O bonds of carbonyl ligands are characterized (*Table 4*) by high values of $\rho_b$ (3.7 eÅ$^{-3}$ av.) and large negative values of $\nabla^2\rho_b$ (– 48 eÅ$^{-5}$ av.). Their large negative $E_b^e$ values (– 8.35 hartree Å$^{-3}$ av.) are due to the larger magnitude of the potential-energy density ($V_b$ = – 13.35 hartree Å$^{-3}$ av.) with respect to the kinetic-energy density ($G_b$ = 4.96 hartree Å$^{-3}$ av.). The above values agree well with the corresponding values found in analogous compounds [7][18] and are very close to those of typical covalent bonds. Unlike the Co–$C_{CO}$ bonds, the topological properties of all the C≡O bonds are very similar, except for the C(4)–O(4) bond that shows slight differences ($R_e$ = 1.174(4), $R_x$ = 0.528 Å, and $\rho_b$ = 3.4(1) eÅ$^{-3}$) with respect to the terminal carbonyl ligands ($R_e$ = 1.136(6), $R_x$ = 0.438 Å av., and $\rho_b$ = 3.8(2) eÅ$^{-3}$ av.).

Although the C(7)=O(7) bond ($R_e$ = 1.209(4) and $R_x$ = 0.547 Å) is formally a double bond and, therefore, longer, it shows critical-point values close to those of the C≡O bonds. The C(6)–O(6) and C(7)–O(6) formal single bonds ($R_e$ = 1.394(4) Å av.

Table 5. *Bond Critical-Point Properties of the Intermolecular Interactions Marked with an Asterisk in* Table 1

| X-Y | $\rho_b$ [eÅ$^{-3}$] | $\nabla^2\rho_b$ [eÅ$^{-5}$] | $\lambda_1$ [eÅ$^{-5}$] | $\lambda_2$ [eÅ$^{-5}$] | $\lambda_3$ [eÅ$^{-5}$] | $G_b$ [hartree Å$^{-3}$] | $G_b/\rho_b$ [hartree e$^{-1}$] | $V_b$ [hartree Å$^{-3}$] | $E_b^e$ [hartree Å$^{-3}$] |
|---|---|---|---|---|---|---|---|---|---|
| O(1′)···O(2′) | 0.03 | 0.47 | −0.08 | −0.06 | 0.61 | 0.02 | 0.81 | −0.02 | 0.00 |
| O(1′)···O(3′) | 0.02 | 0.36 | −0.06 | −0.05 | 0.47 | 0.02 | 0.90 | −0.01 | 0.01 |
| O(1′)···O(6′) | 0.02 | 0.37 | −0.05 | −0.04 | 0.46 | 0.02 | 0.92 | −0.01 | 0.01 |
| O(2′)···O(5′) | 0.03 | 0.39 | −0.06 | −0.05 | 0.50 | 0.02 | 0.68 | −0.01 | 0.01 |
| O(2′)···O(7′) | 0.02 | 0.42 | −0.07 | −0.06 | 0.55 | 0.02 | 1.04 | −0.01 | 0.01 |
| O(3′)···O(6′) | 0.03 | 0.56 | −0.09 | −0.08 | 0.73 | 0.03 | 0.95 | −0.02 | 0.01 |
| O(2′)···C(8) | 0.03 | 0.38 | −0.06 | −0.03 | 0.47 | 0.02 | 0.67 | −0.01 | 0.01 |
| O(4)···C(6′) | 0.05 | 0.71 | −0.13 | −0.04 | 0.88 | 0.04 | 0.77 | −0.03 | 0.01 |
| O(6′)···C(8) | 0.04 | 0.53 | −0.08 | −0.05 | 0.66 | 0.03 | 0.71 | −0.02 | 0.01 |
| O(7′)···C(7) | 0.05 | 0.76 | −0.14 | −0.06 | 0.96 | 0.04 | 0.82 | −0.03 | 0.01 |
| O(7)···C(2′) | 0.07 | 0.74 | −0.13 | −0.03 | 0.90 | 0.04 | 0.63 | −0.04 | 0.00 |
| O(4)···H(8) | 0.04 | 0.55 | −0.11 | −0.11 | 0.77 | 0.03 | 0.74 | −0.02 | 0.01 |
| O(7)···H(9) | 0.05 | 1.21 | −0.17 | −0.15 | 1.53 | 0.06 | 1.24 | −0.04 | 0.02 |

and $R_x = 0.576$ Å av.) show smaller values of $\rho_b$, $\nabla^2\rho_b$, $G_b$, $|V_b|$, and $|E_b^e|$ with respect to the other CO bonds.

*The Co–Co Bond.* The Co–Co bond exhibits a small and positive $\nabla^2\rho_b$ value (2.0(3) eÅ$^{-5}$), close to those found in other compounds. A comparison of $\rho_b$ and of the metal-metal $R_e$ value of **1** ($\rho_b = 0.76(6)$ eÅ$^{-3}$ and Co–Co = 2.4222(3) Å) with the corresponding values of other systems ($[Co_4(CO)_{11}(PPh_3)]$ [19]: $\rho_b = 0.252(3)$ eÅ$^{-3}$ and Co–Co = 2.528(8) Å; $[Co(CO)_3(As(PPh_3)]_2$ [18]: $\rho_b = 0.204(11)$ eÅ$^{-3}$ and Co–Co = 2.6430(2) Å; $[Mn_2(CO)_{10}]$ [7]: $\rho_b = 0.190(4)$ eÅ$^{-3}$ and Mn–Mn = 2.9042(8) Å) shows that the values of $\rho_b$ have the reverse trend with respect to the bond distance $R_e$. The critical point values of the Co–Co bond (see *Table 4*) confirm the 'closed-shell' character of the metal–metal bond in clusters and a flat $\rho(\boldsymbol{r})$ in the internuclear region, as shown by the small absolute values of the $\lambda_1$ and $\lambda_2$ curvatures at the BCP.

The Co–Co bond path is almost linear (see *Fig. 3*, *a* and *b*): the Co–Co BCP is displaced by 0.13 Å from the internuclear axis and in the direction opposite to that claimed by the bent Co–Co bond model [5].

*Hall et al.* [6] found that the amount of direct bonding between the Co-atoms in systems with two bridging ligands increases with the decrease of the dihedral angle between the bridges and with the shortening of the metal–metal bond. Our complex has a smaller dihedral angle (111°) and a shorter Co–Co distance (2.4222(3) Å) as compared to those (129° and 2.5301(8) Å) of $[Co_2(CO)_8]$, where the Co–Co bond was not found.

In complex **1**, the distances (within 0.3 Å) of the Co(1)Co(2)C(4) and Co(1)-Co(2)C(6) ring critical points from the Co–Co BCP suggest a possible coalescence when the metal–metal distance becomes longer, for example as in $[Co_2(CO)_8]$.

*The γ-Lactone Ring*. As expected, all bonds of the γ-lactone ring have high negative Laplacian and $E_b^e$ values, typical of covalent interactions (*Fig. 4*, *c*). The ring BCP is close to the center of the five-membered ring (*Fig. 3*, *c*). Each atom of the ring, with the exception of C(6), has three VSCC maxima disposed at 120° in the direction of the bonds. The C(6) atom has four VSCC maxima approximately disposed at vertices of a

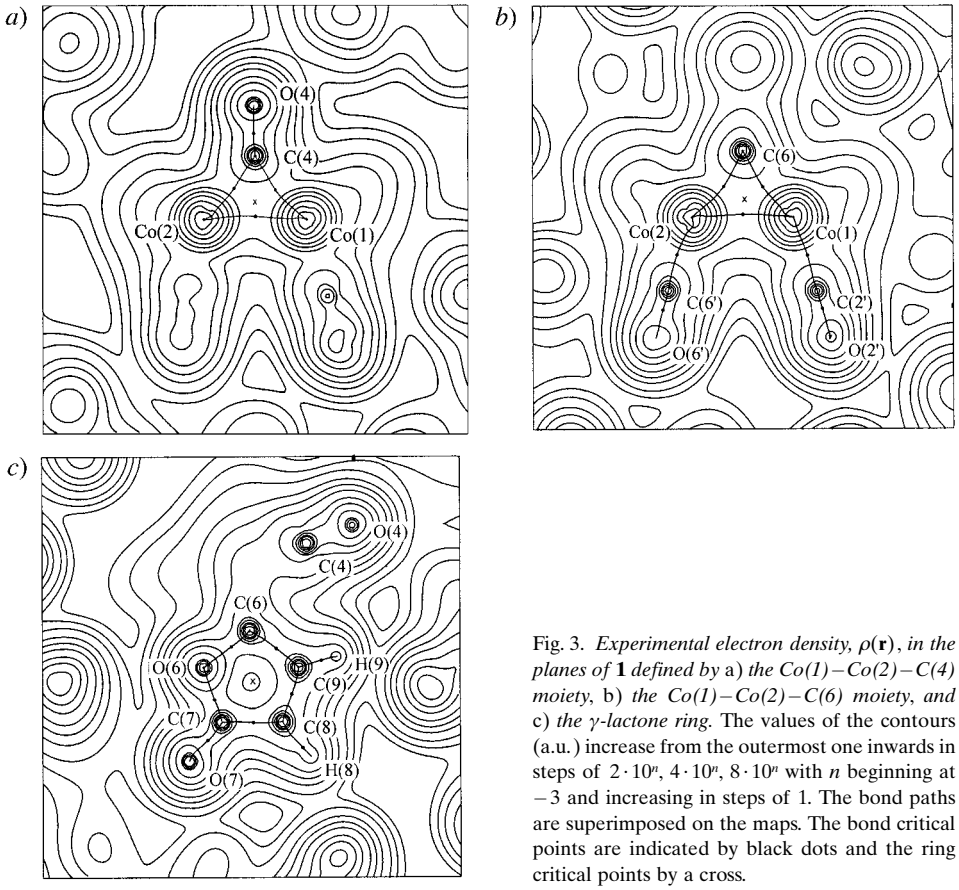


Fig. 3. *Experimental electron density,* $\rho(\mathbf{r})$, *in the planes of* **1** *defined by* a) *the Co(1)–Co(2)–C(4) moiety*, b) *the Co(1)–Co(2)–C(6) moiety, and* c) *the γ-lactone ring.* The values of the contours (a.u.) increase from the outermost one inwards in steps of $2\cdot10^n$, $4\cdot10^n$, $8\cdot10^n$ with $n$ beginning at $-3$ and increasing in steps of 1. The bond paths are superimposed on the maps. The bond critical points are indicated by black dots and the ring critical points by a cross.

tetrahedron; two of these point toward the Co-atoms and the other two are directed toward C(9) and O(6). One of the three VSCC maxima on O(6) is faced to the CO(3′) and CO(7′) carbonyls, and the resulting repulsion between this charge concentration and the $C_{CO}$ atoms may explain the decreasing of the dihedral angle between the two bridges with respect to the corresponding angle in $[Co_2(CO)_8]$.

*Atomic Charges. Table 3* shows that the γ-lactone ring and Co-atoms have zero charges within the experimental errors. As already found in other compounds [7], the CO ligands have a negative charge at the C-atom and a positive charge at the O-atom, and they can be considered neutral within $3\sigma$. In *Fig. 4*, *a* and *b*, the Laplacian trend around the CO ligands shows that the C-centroids of negative charge are shifted toward the Co-atom, indicating the polarization senses of CO molecules. Thus, the effect of the polarization appears to be predominant with respect to the electronegativity of the atoms in the determination of the multipole charges.

2.4. *Intermolecular Interactions.* In *Table 5* are listed the intermolecular interactions for which a bond path was found. They have $\rho_b$ and $\nabla^2\rho_b$ values within the intervals

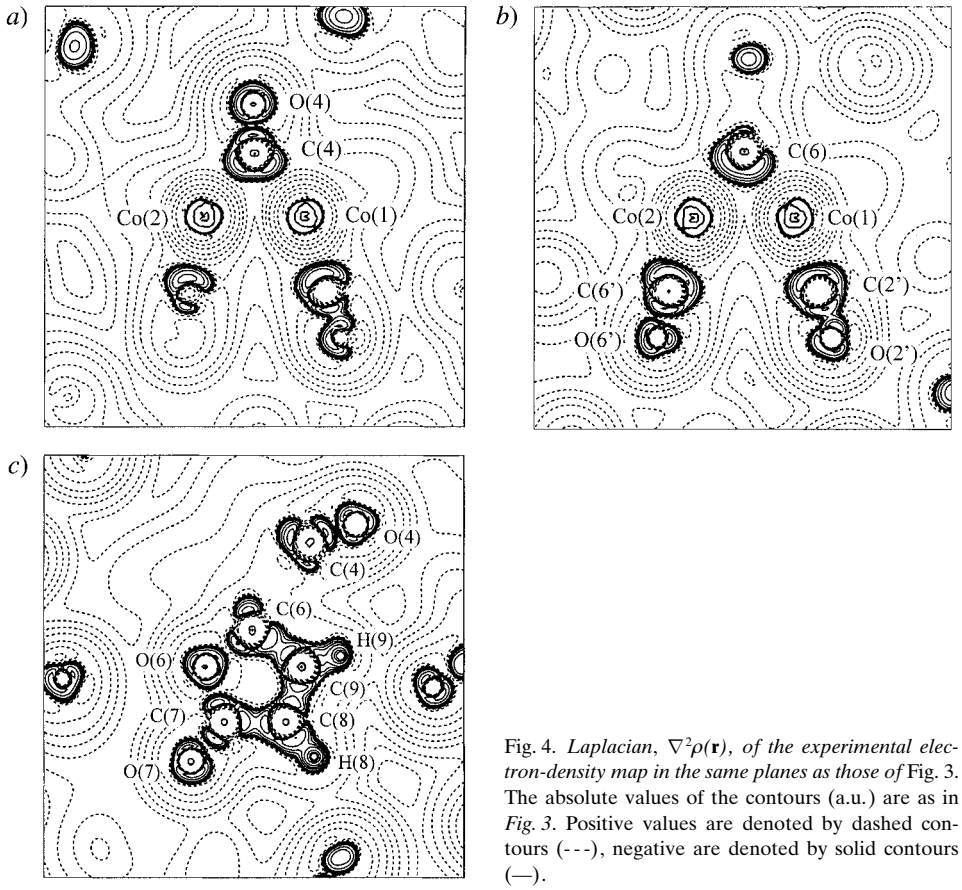


Fig. 4. *Laplacian,* $\nabla^2\rho(\mathbf{r})$*, of the experimental electron-density map in the same planes as those of* Fig. 3. The absolute values of the contours (a.u.) are as in *Fig. 3*. Positive values are denoted by dashed contours (- - -), negative are denoted by solid contours (—).

0.02 – 0.07 eÅ$^{-3}$ and 0.36 – 1.21 eÅ$^{-5}$, respectively. Even if these ranges of values are at limit of the experimental accuracy, the POP model appears capable of reproducing the effects of intermolecular interactions. In fact, the BCP properties of the weak interactions O ··· O and O ··· C reported in *Table 5* are very close to the corresponding properties observed for $[Mn_2(CO)_{10}]$ [7b].

The H(8) and H(9) atoms form two H-bonds with O(4) and O(7), respectively (O(7) ··· H(9) 2.32 Å, O(7) ··· C(9) 3.175 Å, H(9) ··· O(7) – C(7) 121°; O(4) ··· H(8) 2.55 Å, O(4) ··· C(8) 3.542 Å, H(8) ··· O(4) – C(4) 128°). In the crystal packing (*Fig. 5*,*a*), the molecules, connected through the H-bonds, form waving ribbons along the [010] direction; the ribbons are joined *via* O ··· O interactions, forming (*h*00) planes. In fact, the crystals are easily splitted into laminae along the (100) face.

The experimental electron density from the POP model appears to be more polarized along the O(7) ··· H(9) bond in comparison to that from the IAM model (*Fig. 5*,*b* and *c*). The same trend is observed for the O(4) ··· H(8) bond. The C – H ··· O bonds reflect the characteristics of the ionic interaction, and their BCP properties are in

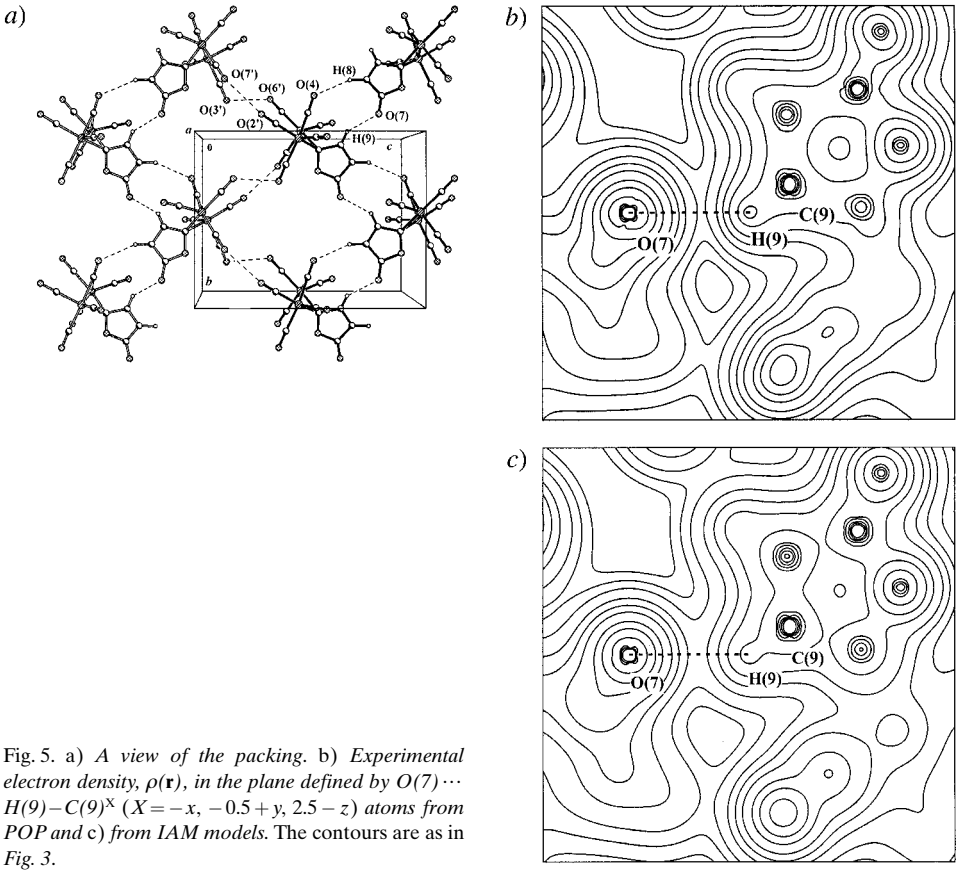


Fig. 5. a) *A view of the packing.* b) *Experimental electron density, $\rho(\mathbf{r})$, in the plane defined by O(7)⋯H(9)–C(9)$^X$ ($X = -x, -0.5+y, 2.5-z$) atoms from POP and* c) *from IAM models.* The contours are as in *Fig. 3*.

noticeable agreement with those present in lithium bis(tetramethylammonium)hexanitrocobaltate(III) [20].

The VSCC maxima around the atoms involved in the intermolecular interactions, showed in *Table 1*, avoid the interaction directions.

**3. Discussion.** – Our electron-density study of $[Co_2(CO)_6(\mu\text{-}CO)(\mu\text{-}C_4O_2H_2)]$ (**1**) gives, for the first time, an experimental evidence for the existence of a Co–Co bond in a system with bridging ligands. The question of a direct metal-metal interaction for this interesting class of compounds has been answered definitely by this study. The topological properties at BCPs of the Co–Co and Co–$C_{CO}$ bonds are in close agreement with those found for Mn–Mn and Mn–$C_{CO}$ bonds in $[Mn_2(CO)_{10}]$ and confirm the classification of the bonding interactions we previously proposed [7b] for organometallic and coordination compounds. The critical-point properties of the O⋯O and O⋯C interactions in complex **1** are very similar to those observed before for these kind of contacts in $[Mn_2(CO)_{10}]$, thus this agreement reinforces the ability of the POP model to describe also these very weak interactions.

The topological analysis shows the presence of two ionic H-bonds that contribute, together with the O···O interactions, to stabilize the crystal structure. It is worth stressing that such subtle, yet typical bonding features are still observable in systems where the scattering is dominated by the heavy metal atoms.

The authors wish to dedicate the paper to Prof. *László Markó*, who supplied the crystals, for remembering the long collaboration with one of them (*G. G.*). We thank *M. U. R. S. T.* (Cofin98) for financial support.

## Experimental Part

*Data Collection and Reduction. μ-Carbonylhexacarbonyl[μ-(5-oxofuran-2(5H)-ylidene-κC:κC)]dicobalt* (Co–Co) (**1**; $[Co_2(CO)_6(\mu\text{-}CO)(\mu\text{-}C_4O_2H_2)]$), $M_r$ 395.99, crystallizes in the orthorhombic space group $P2_12_12_1$: $a = 9.769(2)$ Å, $b = 10.488(2)$ Å, $c = 13.787(3)$ Å, $V = 1413.6(5)$ Å$^3$, $Z = 4$, $D_x = 1.861$ g/cm$^3$, $\mu = 2.388$ mm$^{-1}$, $F(000) = 776$. A red crystal was put in a *Lindemann* glass capillary, and the intensity data were collected with graphite-monochromatized Mo$K_\alpha$ radiation ($\lambda$ 0.71073 Å) with $\theta$-$2\theta$ scan method on a *Siemens-P4* diffractometer equipped with a $N_2$ gas stream low temperature device. The crystal was cooled to 150 K within nearly 3 h; 8960 reflections were collected up to $2\theta = 100°$ (limiting indices $0 < h < 21$, $0 < k < 22$, $0 < l < 29$), scan width = 2.2° and variable scan speed (1.50–15.00°/min). Two standard reflections were measured every 50 reflections, and no crystal decay occurred. The intensities were corrected for absorption [21]. Data reduction was made with P3 and SHELXS programs [22]. The independent reflections were 7631 ($R_{int} = \Sigma||F_o|^2 - |F_o|^2(\text{mean})|/\Sigma|F_o|^2 = 0.022$), $R_\sigma = \Sigma[\sigma(|F_o|^2)]/\Sigma[|F_o|^2] = 0.043$).

*Refinements.* Conventional refinement (independent-atom model, IAM) of the positional parameters of all atoms, of anisotropic displacement parameters for Co-, C-, and O-atoms, and of isotropic ones for H-atoms converged at $R = 0.0414$. Atomic scattering factors including those for anomalous scattering of the Co-, C-, and O-atoms were taken from the 'International Tables for Crystallography (1995, vol. C). The data were corrected for isotropic extinction as determined by least-squares refinement ($y_{min} = 0.8$, $y = (|F_o|/|F_{corr}|)$. The quantity minimized was $\Sigma w(|F_o|^2 - k^2|F_c|^2)^2$ based on 6072 independent reflections with $I > 2\sigma(I)$ and weights $w = 1/\sigma^2(F_o^2)$. Further information on IAM refinement: $N_o$ (no. of reflections) = 6072, $N_p$ (no. of parameters) = 207, $R(F) = \Sigma||F_o| - k|F_c||/\Sigma|F_o| = 0.0414$, $wR(F) = [\Sigma w(|F_o| - k|F_c|^2)/\Sigma w|F_o|^2]^{1/2} = 0.0534$, $R(F^2) = \Sigma||F_o|^2 - k^2|F_c|^2|/\Sigma|F_o|^2 = 0.0696$, $wR(F^2) = [\Sigma w(|F_o|^2 - k^2|F_c|^2)^2/\Sigma w|F_o|^4]^{1/2} = 0.0933$, $S = [\Sigma w(|F_o|^2 - k^2|F_c|^2)^2/(N_o\text{-}N_p)]^{1/2} = 1.387$, $k$ (scale factor) = 1.892(2), $(\text{shift/e.s.d.})_{max} = 0.03$.

The Co-, C- and O-parameters from the conventional refinement were used as starting values for the multipole refinement by the aspherical atom formalism developed by Stewart [9]. H-Atom positions were fixed to those obtained by a previous multipole refinement, where the H-atoms are polarized in the direction of the atom to which they are bonded, and only their isotropic thermal parameters were refined. The rigid pseudo-atom model is now well-established as the most effective tool for electron-density studies, and the basic equations of the formalism are readily accessible. The following rigid pseudo-atom model (POP) was adopted: the nucleus and the spherical core electron density correspond to the IAM, and the deformation density is a sum of terms expressed by $C_{nlm}R_n(r)Y_{lm}(\theta,\varphi)$, where $C_{nlm}$ is a population parameter, $R_n(r)$ is a radial function of the *Slater* type or a fixed linear combination of exponentials, and $Y_{lm}(\theta,\varphi)$ is a surface spherical harmonic. A monopole deformation has spherical symmetry and confers a net charge to the pseudo-atom. All higher multipole terms cause aspherical deformations of the pseudo-atom, but have no effect on the net charge. On the Co-atom position, functional expansions up to the hexadecapole level were introduced, whereas the expansions were broken at the octapole level at the C- and O-positions and at the dipole level for the H-atoms. For the Co-, O-, C-, and H-atoms, the core and valence monopole scattering factors were calculated from *Hartree-Fock* atomic wave functions [23a]. A single parameter was refined for the core of all C- and O-atoms. The plane containing the γ-lactone ring of the title compound is a molecular symmetry plane, and hence only two valence monopole parameters were varied, for the C- and O-atoms of the carbonyls, resp., while the three monopole parameters of one Co-atom were considered equal to those of the other. Each H monopole was a single shell, given by $\exp(-2.48r)$. For the higher multipoles, the *Slater*-type exponents, $\alpha$s, of O-, C- and H-atoms were assigned fixed values based on theory [23b] and the $\alpha$s of the Co-atoms were determined in the least-squares refinement. To test the effect of the anharmonicity in the thermal motion, we introduced third-order *Gram-Charlier* [24] coefficients in the least-squares procedure. Introduction of anharmonic parameters led only to a marginal drop in the $R$ factor, but no significant improvement in the multipole analysis, so they were excluded

from the final model. All refinements were carried out with the VALRAY program implemented by *Stewart* and *Spackman* [25]. A list of all refined parameters is given as Supporting Information.

*Hirshfeld's* rigid-bond test [26] was applied to the final thermal parameters. The r.m.s. of the mean-square displacement amplitude for bonded atoms along the bond vector in **1** was 0.001 Å; therefore, the final model is consistent with the rigid-bond hypothesis. Information on the multipole refinement: $N_o = 6072$, $N_p = 571$, $R(F) = 0.0285$, $wR(F) = 0.0412$, $R(F^2) = 0.0385$, $wR(F^2) = 0.0687$, $S = 1.053$, $k = 0.891(5)$, $(\text{shift/e.s.d.})_{max} = 0.02$.

Crystallographic data (excluding structure factors) for the structure reported in this paper have been deposited with the *Cambridge Crystallographic Data Centre* as deposition No. CCDC 152323. Copies of the data can be obtained, free of charge, on application to the CCDC, 12 Union Road, Cambridge CB2 1EZ, UK (fax: +44(1223) 336033; e-mail: deposit@ccdc.cam.ac.uk).

## REFERENCES


[1] G. Gardner Sumner, H. P. Klug, L. E. Alexander, *Acta Crystallogr.* **1964**, *17*, 732; G. Braterman, *Struct. Bonding (Berlin)* **1972**, *10*, 57.

[2] D. L. Thorn, R. Hoffmann, *Inorg. Chem*. **1978**, *17*, 126; R. H. Summerville, R. Hoffmann, *J. Am. Chem. Soc*. **1979**, *101*, 3821; W. Heijser, E. J. Baerends, P. Ros, *Faraday Symp. Chem. Soc*. **1980**, *14*, 211.

[3] H.-J. Freund, G. Hohneicher, *Theor. Chim. Acta (Berlin)* **1979**, *52*, 145; H.-J. Freund, B. Dick, G. Hohneicher, *Theor. Chim. Acta (Berlin)* **1980**, *57*, 181.

[4] P. C. Leung, P. Coppens, *Acta Crystallogr., Sect. B* **1983**, *39*, 535.

[5] A. A. Low, K. L. Kunze, P. J. MacDougall, M. B. Hall, *Inorg. Chem*. **1991**, *30*, 1079.

[6] A. A. Low, M. B. Hall, *Inorg. Chem*. **1993**, *32*, 3880.

[7] a) R. Bianchi, G. Gervasio, D. Marabello, *Chem. Commun*. **1998**, 1535; b) R. Bianchi, G. Gervasio, D. Marabello, *Inorg. Chem*. **2000**, *39*, 989.

[8] a) R. F. W. Bader, 'Atoms in Molecules – a Quantum Theory', Oxford Univ. Press, Oxford, 1990; b) R. F. W. Bader, *J. Phys. Chem. A* **1998**, *102*, 7314; b) R. F. W. Bader, *J. Phys. Chem. A* **1998**, *102*, 7314; c) R. F. W. Bader, P. J. MacDougall, C. D. H. Lau, *J. Am. Chem. Soc*. **1984**, *106*, 1594.

[9] R. F. Stewart, *Acta Crystallogr., Sect. A* **1976**, *32*, 565.

[10] O. S. Mills, G. Robinson, *Inorg. Chim. Acta* **1967**, *1*, 61.

[11] R. Perlaki, L. Markó, G. Gervasio, E. Sappa, G. Pályi, *J. Organomet. Chem*. **1995**, *502*, 25.

[12] L. Markó, G. Gervasio, S. Vastag, *J. Cluster Sci*. **1996**, *7*, 423.

[13] L. Markó, G. Gervasio, D. Marabello, unpublished results.

[14] H. W. Sternberg, J. G. Shukys, C. Delle Donne, R. Markby, R. A. Friedel, I. Wender, *J. Am. Chem. Soc*. **1959**, *81*, 2339.

[15] G. Pályi, G. Váradi, L. Markó, 'Stereochemistry of Organometallic and Inorganic Compounds', Ed. Bernal I., Elsevier, Amsterdam-Oxford-New York-Tokio, 1986, Vol. 1, p. 358.

[16] Yu. A. Abramov, *Acta Crystallogr., Sect. A* **1997**, *53*, 264.

[17] E. Espinosa, E. Molins, C. Lecomte, *Chem. Phys. Lett*. **1998**, *285*, 170.

[18] P. Macchi, D. M. Proserpio, A. Sironi, *J. Am. Chem. Soc*. **1998**, *120*, 13429.

[19] P. Macchi, L. Garlaschelli, S. Martinengo, A. Sironi, *J. Am. Chem. Soc*. **1999**, *121*, 10428.

[20] R. Bianchi, C. Gatti, V. Adovasio, M. Nardelli, *Acta Crystallogr., Sect. B* **1996**, *52*, 471.

[21] A. C. T. North, D. C. Phillips, F. S. Mathews, *Acta Crystallogr., Sect. A* **1968**, *24*, 351.

[22] G. M. Sheldrick 'SHELXTL IRIS', Siemens Analytical X-Ray Instruments Inc., Madison, WI, 1990.

[23] a) E. Clementi, C. Roetti, *At. Data and Nucl. Data Tables* **1974**, *14*, 177; b) W. J. Hehre, R. Ditchfield, R. F. Stewart, J. A. Pople, *J. Chem. Phys.* **1970**, *52*, 2769.

[24] C. K. Johnson, H. A. Levy, 'International Tables of X-Ray Crystallography', Kynoch Press, Birmingham, 1974, Vol. IV, p. 311–316.

[25] R. F. Stewart, M. A. Spackman, 'VALRAY User's Manual, 1983', Department of Chemistry, Carnegie-Mellon University, Pittsburgh.

[26] F. L. Hirshfeld, *Acta Crystallogr., Sect. A* **1976**, *32*, 239.


*Received November 13, 2000*